

Attenuation of small-amplitude oscillations in a prominence-corona model with a transverse magnetic field

R. Soler, R. Oliver and J. L. Ballester

Departament de Física, Universitat de les Illes Balears, E-07122, Palma de Mallorca, Spain

Abstract

Observations show that small-amplitude prominence oscillations are usually damped after a few periods. This phenomenon has been theoretically investigated in terms of non-ideal magnetoacoustic waves, non-adiabatic effects being the best candidates to explain the damping in the case of slow modes. We study the attenuation of non-adiabatic magnetoacoustic waves in a slab prominence embedded in the coronal medium. We assume an equilibrium configuration with a transverse magnetic field to the slab axis and investigate wave damping by thermal conduction and radiative losses. The magnetohydrodynamic equations are considered in their linearised form and terms representing thermal conduction, radiation and heating are included in the energy equation. The differential equations that govern linear slow and fast modes are numerically solved to obtain the complex oscillatory frequency and the corresponding eigenfunctions. We find that coronal thermal conduction and radiative losses from the prominence plasma reveal as the most relevant damping mechanisms. Both mechanisms govern together the attenuation of hybrid modes, whereas prominence radiation is responsible for the damping of internal modes and coronal conduction essentially dominates the attenuation of external modes. In addition, the energy transfer between the prominence and the corona caused by thermal conduction has a noticeable effect on the wave stability, radiative losses from the prominence plasma being of paramount importance for the thermal stability of fast modes. We conclude that slow modes are efficiently damped, with damping times compatible with observations. On the contrary, fast modes are less attenuated by non-adiabatic effects and their damping times are several orders of magnitude larger than those observed. The presence of the corona causes a decrease of the damping times with respect to those of an isolated prominence slab, but its effect is still insufficient to obtain damping times of the order of the period in the case of fast modes.

Key words: Sun: oscillations, Sun: magnetic fields, Sun: corona, Sun: prominences
PACS: 52.35.Bj, 96.60.P-

1 Introduction

Solar prominences are large-scale coronal magnetic structures whose material, cooler and denser than the typical coronal medium, is in plasma state. Prominences are supported against gravity by the coronal magnetic field, which also maintains the prominence material thermally isolated from the corona. Small-amplitude oscillations in solar prominences were detected almost 40 years ago (Harvey, 1969). These oscillatory motions seem to be of local nature and their velocity amplitude is typically less than $2\text{--}3\text{ km s}^{-1}$. Observations have also allowed to measure a wide range of periods between 30 s (Balthasar et al., 1993) and 12 h (Foullon et al., 2004). More recently, some high-resolution observations of prominence oscillations by the Hinode/SOT instrument have been reported (Okamoto et al., 2007; Berger et al., 2008; Ofman & Wang, 2008). From the theoretical point of view, the oscillations have been interpreted by means of the magnetoacoustic eigenmodes supported by the prominence body. A recent example is the work by Terradas et al. (2008) in which the observations of Okamoto et al. (2007) are interpreted as fast kink waves. The reader is referred to Oliver & Ballester (2002); Ballester (2006); Banerjee et al. (2007) for extensive reviews of both observational and theoretical studies.

Evidence of the attenuation of small-amplitude prominence oscillations has been reported in some works (Molowny-Horas et al., 1999; Terradas et al., 2002; Lin, 2004). A typical feature of these observations is that the oscillatory motions disappear after a few periods, hence they are quickly damped by one or several mechanisms. The theoretical investigation of this phenomenon in terms of magnetohydrodynamic (MHD) waves has been broached by some authors by removing the ideal assumption and by including dissipative terms in the basic equations. Non-adiabatic effects appear to be very efficient damping mechanisms and have been investigated with the help of simple prominence models (Ballai, 2003; Carbonell et al., 2004, 2006; Terradas et al., 2005). Nevertheless, other damping mechanisms have been also proposed, like wave leakage (Schutgens, 1997a,b; Schutgens & Toth, 1999), dissipation by ion-neutral collisions (Forteza et al., 2007) and resonant absorption (Arregui et al., 2008).

In a previous work (Soler et al., 2007, hereafter Paper I), we have studied for the first time the wave attenuation by non-adiabatic effects of a prominence slab embedded in the corona. In that work the magnetic field is parallel to the slab axis and it is found that the corona has no influence on the internal slow modes, but it is of paramount importance to explain the damping of fast modes, which are more attenuated than in simple models that do not consider the coronal medium. Following the path initiated in Paper I, here we investi-

Email address: [roberto.soler,ramon.oliver,joseluis.ballester]@uib.es
(R. Soler, R. Oliver and J. L. Ballester).

gate the wave damping due to non-adiabatic mechanisms (radiative losses and thermal conduction) in an equilibrium made of a prominence slab embedded in a coronal medium, but now we consider a magnetic field transverse to the slab axis. This configuration and that studied in Paper I correspond to limit cases, since measurements with Zeeman and Hanle effects indicate that the magnetic field lines are skewed to the long axis of prominences. On average, the prominence axis and the magnetic field form an angle of about 20 deg. Thus, the skewed case is relegated to a future investigation.

The equilibrium configuration assumed here was analysed in detail by Joarder & Roberts (1992) and Oliver et al. (1993) in the case of ideal, adiabatic perturbations. The main difference between both works is in the treatment of gravity. Joarder & Roberts (1992) neglected the effect of gravity and so straight field lines were considered. On the other hand, Oliver et al. (1993) took gravity into account and assumed curved field lines according to the Kippenhahn & Schölter (1957) model modified to include the surrounding coronal plasma (Poland & Anzer, 1971). Despite this difference, both studies agree in establishing a distinction between different normal modes depending on the dominant medium supporting the oscillation. Hence, internal modes are essentially supported by the prominence slab whereas external modes arise from the presence of the corona. In addition, hybrid (or string) modes appear due to the combined effect of both media.

The investigation of the thermal attenuation of oscillations supported by such equilibrium is unsettled to date and, indeed, this is the main motivation for the present study. However, two works (Terradas et al., 2001, 2005) studied the wave damping in an isolated prominence slab. Terradas et al. (2001) considered radiative losses given by the Newtonian law of cooling as damping mechanism and studied the attenuation in the Kippenhahn & Schölter (1957) and Menzel (1951) prominence models. Subsequently, Terradas et al. (2005) considered a more complete energy equation including optically thin radiation, plasma heating and parallel thermal conduction, and assumed straight field lines since gravity was neglected. The main conclusion of both works is that non-adiabatic mechanisms are only efficient in damping slow modes whereas fast modes remain almost undamped. Nevertheless, in the light of the results of Paper I, the presence of the coronal medium can have an important repercussion on the wave damping. The investigation of this effect is the main aim of the present work. Therefore, we extend here the work of Terradas et al. (2005) by considering the presence of the corona and neglect the effect of gravity as in Joarder & Roberts (1992) for simplicity.

This paper is organised as follows. Section 2 contains a description of the equilibrium configuration and the basic equations which govern non-adiabatic magnetoacoustic waves. Then, the results of this work are extensively discussed in Sect. 3. Finally, our conclusions are given in Sect. 4.

2 Equilibrium and basic equations

The equilibrium configuration (see Fig. 1) is made of a homogeneous plasma slab with prominence conditions (density ρ_p and temperature T_p), whose axis is orientated along the z -direction, embedded in a coronal environment (density ρ_c and temperature T_c). The system is bounded in the x -direction due to the presence of two rigid walls representing the solar photosphere, but it is unlimited in the y - and z -directions. The width of the prominence slab is $2x_p$ and the total width of the system is $2x_c$. The magnetic field is transverse to the prominence slab, $\vec{B}_0 = B_0 \hat{e}_x$, with B_0 everywhere constant.

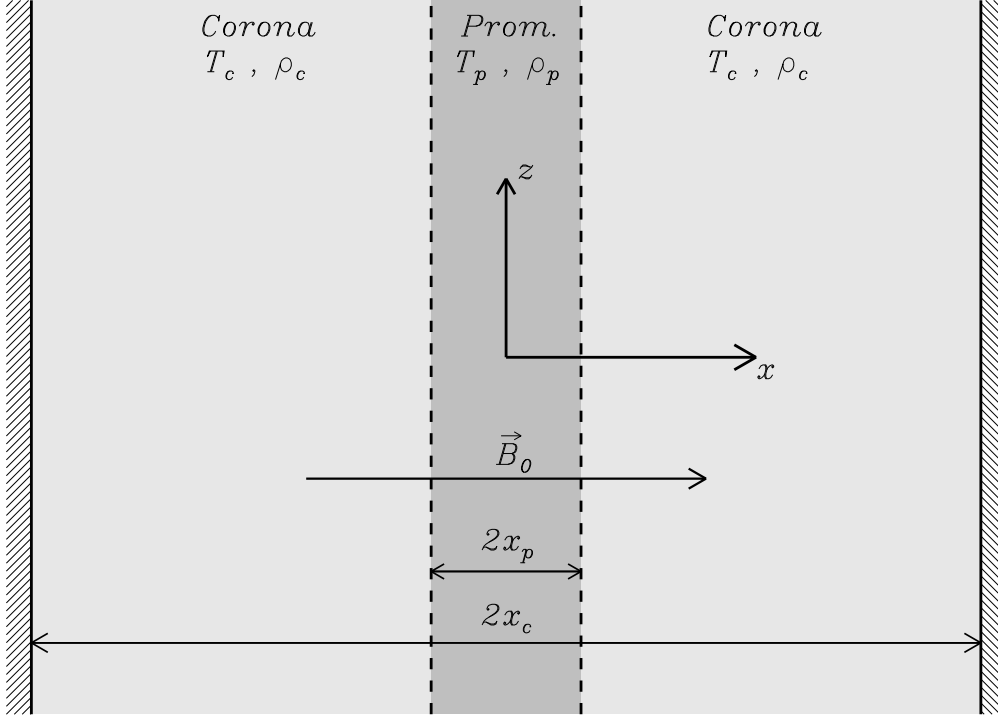


Fig. 1. Sketch of the equilibrium. The dark region represents the prominence slab while the light region corresponds to the corona. The photospheric walls are the two hatched areas on both sides of the corona.

In order to find the basic equations that govern non-adiabatic magnetoacoustic waves we follow the same process as in Terradas et al. (2005). We consider the usual MHD equations (Eqs. (1)–(6) of Terradas et al., 2005) in which non-adiabatic terms have been included in the energy equation,

$$\frac{Dp}{Dt} - \frac{\gamma p}{\rho} \frac{D\rho}{Dt} + (\gamma - 1)[\rho L(\rho, T) - \nabla \cdot (\vec{\kappa} \cdot \nabla T)] = 0, \quad (1)$$

where p , ρ and T are the gas pressure, density and temperature, respectively. The quantity γ is the adiabatic ratio, here taken $\gamma = 5/3$. The non-ideal terms in Eq. (1) are explained in detail in Carbonell et al. (2004). Thermal

conduction is represented by $\nabla \cdot (\vec{\kappa} \cdot \nabla T)$, where $\vec{\kappa}$ is the conductivity tensor which in coronal and prominence applications is usually approximated by its parallel component to the magnetic field, $\kappa_{\parallel} = 10^{-11} T^{5/2} \text{ W m}^{-1} \text{ K}^{-1}$. Radiative losses and heating are evaluated together through the heat-loss function, $L(\rho, T) = \chi^* \rho T^{\alpha} - h \rho^a T^b$, where radiation is parametrised with χ^* and α (see Table I of Paper I) and the heating scenario is given by exponents a and b (Rosner et al., 1978; Dahlburg & Mariska, 1988).

Regarding our equilibrium configuration, the reader must be aware that, although there have been some attempts to construct a self-consistent prominence model including both magnetostatics and thermodynamics (e.g. Milne et al., 1979; Low & Wu, 1981; Anzer & Heinzel, 1999), to date this task remains to be done. Here, we consider a simplified prominence-corona configuration, but it includes the two basic ingredients observed in real prominences. First, the existence of a steep temperature gradient between the prominence and the corona and, second, the apparent thermal isolation of the prominence material from the much hotter corona. The first point is addressed by considering that the temperature profile is a step function, and so the prominence-corona transition region (PCTR) has not been considered. This choice is supported by results of previous works (e.g. Oliver & Ballester, 1996) which showed that the PCTR has a minor influence on the prominence oscillatory modes. On the other hand, to represent the thermal isolation we have neglected the heat flux due to thermal conduction at the boundary between the prominence and the corona. Therefore, we impose that both the prominence and the corona are isothermal and thermally isolated, and so radiative losses and heating are locally balanced, i.e. $L(\rho_0, T_0) = 0$, where ρ_0 and T_0 are the local equilibrium density and temperature, respectively.

Assuming that the plasma is at rest in the equilibrium state (i.e. no flux of material) and considering small perturbations, we find the linearised version of the MHD equations (Eqs. (10)–(15) of Terradas et al., 2005). According to the geometry of our model, we assume perturbations of the form $f_1(x) \exp i(\omega t + k_y y + k_z z)$ and exclude Alfvén waves from this analysis by considering only motions and propagation in the xz -plane ($v_y = 0$, $k_y = 0$). Now we combine the resultant expressions and eliminate all the perturbed quantities in favour of the velocity perturbations, v_x and v_z , and the temperature perturbation, T_1 . By this process, we obtain three coupled ordinary differential equations,

$$c_s^2 \frac{d^2 v_x}{dx^2} + \gamma \omega^2 v_x + i k_z c_s^2 \frac{dv_z}{dx} - \frac{i \omega c_s^2}{T_0} \frac{dT_1}{dx} = 0, \quad (2)$$

$$v_A^2 \frac{d^2 v_z}{dx^2} + \left[\omega^2 - k_z^2 \left(v_A^2 + \frac{c_s^2}{\gamma} \right) \right] v_z + i k_z \frac{c_s^2}{\gamma} \frac{dv_x}{dx} + \omega k_z \frac{c_s^2}{\gamma} \frac{T_1}{T_0} = 0, \quad (3)$$

$$\kappa_{\parallel} \frac{1}{p_0} \frac{d^2 T_1}{dx^2} - \left(\omega_T + \frac{i\omega}{\gamma - 1} \right) \frac{T_1}{T_0} - \left(1 + \frac{i\omega_{\rho}}{\omega} \right) \frac{dv_x}{dx} - ik_z \left(1 + \frac{i\omega_{\rho}}{\omega} \right) v_z = 0, \quad (4)$$

where $c_s^2 = \frac{\gamma p_0}{\rho_0}$ is the adiabatic sound speed squared whereas $v_A^2 = \frac{B_0^2}{\mu \rho_0}$ is the Alfvén speed squared. p_0 and B_0 denote the equilibrium gas pressure and magnetic field strength, respectively, and μ is the magnetic permittivity ($\mu = 4\pi 10^{-7}$ in MKS units). Quantities ω_T and ω_{ρ} are defined as follows,

$$\omega_{\rho} \equiv \frac{\rho_0}{p_0} (L + \rho_0 L_{\rho}), \quad \omega_T \equiv \frac{\rho_0}{p_0} T_0 L_T,$$

L_{ρ} , L_T being the partial derivatives of the heat-loss function with respect to density and temperature, respectively,

$$L_{\rho} \equiv \left(\frac{\partial L}{\partial \rho} \right)_T, \quad L_T \equiv \left(\frac{\partial L}{\partial T} \right)_{\rho}.$$

Equations (2), (3) and (4) govern fast and slow magnetoacoustic waves together with the thermal or condensation mode. In this work we do not study the thermal wave since we pay our attention to the magnetoacoustic modes. Terradas et al. (2005) found an approximate analytical solution of Eqs. (2)–(4) by neglecting thermal conduction, a valid assumption in prominence plasmas. However, thermal conduction has an important role in coronal conditions and cannot be neglected in order to perform a realistic description of the oscillatory modes supported by our equilibrium configuration. Hence, we solve the full set of Eqs. (2)–(4) using the numerical code PDE2D (Sewell, 2003) based on finite elements (see Terradas et al., 2005, for an explanation of the method). The jump conditions at the interface between the prominence and the corona are automatically well-treated by the code. These jump conditions are (Goedbloed & Poedts, 2004):

$$[\vec{v}] = \vec{0}, \quad [\vec{B}] = \vec{0}, \quad [p] = 0, \quad (5)$$

where \vec{v} and \vec{B} are the perturbed velocity and the magnetic field vectors, respectively. For a complete closure of the system we need to supply a physically consistent set of boundary conditions for the perturbations at the photospheric walls, $x = \pm x_c$. In this work, we consider two different sets of boundary conditions,

$$v_x = v_z = T_1 = 0, \text{ at } x = \pm x_c, \quad (6)$$

163 and

$$164 \quad v_x = v_z = T_1' = 0, \text{ at } x = \pm x_c, \quad (7)$$

165 where ' indicates derivative with respect to x . Both sets consider line-tied
 166 conditions for the velocity perturbations, i.e. the disturbances are unable to
 167 perturb the dense photospheric plasma which acts as perfectly rigid wall. On
 168 the other hand, sets (6) and (7) differ by the condition for T_1 , which has
 169 different physical implications. Set (6) assumes that the perturbation to the
 170 temperature vanishes at $x = \pm x_c$ and this means that the photospheric walls
 171 are taken as isothermal. On the contrary, set (7) considers a zero-temperature
 172 gradient for the perturbation between the corona and the photosphere, so no
 173 perturbed heat flux is allowed at the boundaries. From our point of view,
 174 set (6) makes more physical sense than set (7), since one can expect that the
 175 much denser photospheric plasma can instantaneously radiate away any in-
 176 coming perturbed heat flux from the corona. However, set (7) imposes that
 177 there is no heat exchange between the corona and the photosphere, although
 178 the temperature perturbation can have a non-zero value at the walls. Regarding
 179 these boundary conditions, Cargill & Hood (1989) performed a study of
 180 the thermal stability of wave and thermal modes in a Cartesian coronal slab
 181 and pointed out that the solutions computed by assuming the boundary con-
 182 ditions given by set (6) are more thermally stable than those obtained for
 183 boundary conditions of set (7).

184 For a fixed real k_z , the numerical solution of Eqs. (2), (3) and (4) provides
 185 with a complex frequency, $\omega = \omega_R + i\omega_I$. In the ideal, adiabatic case $\omega_I = 0$ and
 186 therefore the solutions of Eqs. (2), (3) and (4) are those of Joarder & Roberts
 187 (1992). Using the real and imaginary parts of the frequency, we can com-
 188 pute the oscillatory period, P , the damping time, τ_D , and the ratio of both
 189 quantities,

$$190 \quad P = \frac{2\pi}{\omega_R}, \quad \tau_D = \frac{1}{\omega_I}, \quad \frac{\tau_D}{P} = \frac{1}{2\pi} \frac{\omega_R}{\omega_I}. \quad (8)$$

191 3 Results

192 Unless otherwise stated, the following equilibrium parameters are considered in
 193 all computations: $T_p = 8000$ K, $\rho_p = 5 \times 10^{-11}$ kg m $^{-3}$, $T_c = 10^6$ K, $\rho_c = 2.5 \times$
 194 10^{-13} kg m $^{-3}$, $B_0 = 5$ G, $x_p = 3000$ km and $x_c = 10x_p$. The coronal density is
 195 computed by fixing the coronal temperature and imposing pressure continuity
 196 across the interfaces. In addition, we assume an optically thin prominence
 197 plasma (regime Prominence (1) of Paper I) and a constant heating per unit
 198 volume ($a = b = 0$). In all the following expressions, subscript 0 indicates

199 local equilibrium values, while subscripts p and c denote quantities explicitly
 200 computed with prominence and coronal parameters, respectively.

201 3.1 Dispersion diagram and wave modes

202 Solutions of Eqs. (2)–(4) can be grouped in internal, external and hybrid
 203 modes. Although there is an infinite number of harmonics for internal and
 204 external modes, only two hybrid modes are possible: the hybrid slow mode
 205 and the hybrid fast mode (this nomenclature is taken from Oliver et al., 1993).
 206 Figure 2 shows the dimensionless real part of the frequency versus $k_z x_p$ for
 207 the fundamental symmetric oscillatory modes (i.e. solutions with v_x even with
 208 respect $x = 0$) and some of their harmonics, where we have assumed the
 209 boundary conditions given by Eq. (6). A similar diagram can be obtained for
 210 the antisymmetric modes (i.e. solutions with v_x odd with respect $x = 0$) and
 211 for the other set of boundary conditions (Eq. (7)).

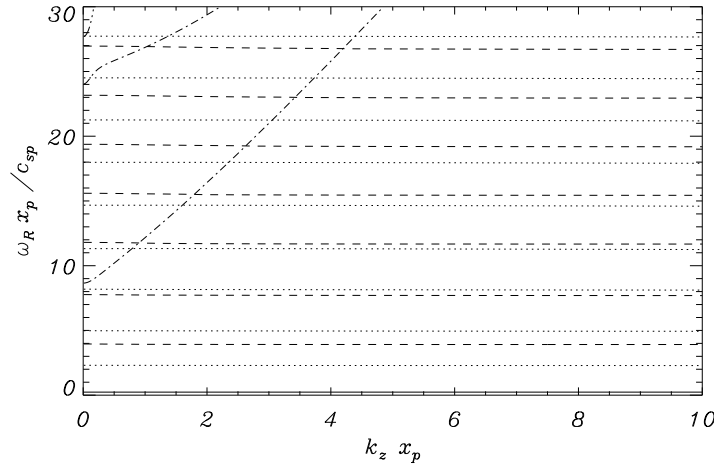


Fig. 2. Dimensionless real part of the frequency versus $k_z x_p$ for the oscillatory symmetric modes: hybrid slow (solid line at the bottom), fundamental internal slow and first harmonics (dotted lines), fundamental external slow and first harmonics (dashed lines), fundamental internal fast and first harmonic (dash-dotted lines) and fundamental external fast (three dot-dashed line at the upper left corner).

212 The behaviour of the real part of the frequency is the same as that explained
 213 by Oliver et al. (1993). The value of ω_R for both internal and external slow
 214 modes and for the hybrid slow mode shows a very weak dependence on k_z
 215 since almost horizontal lines are seen in Fig. 2. On the contrary, both internal
 216 and external fast modes show a quasi-parabolic dependence on k_z (this is
 217 also applicable to the hybrid fast mode, present in the dispersion diagram for
 218 antisymmetric modes). The reader is referred to Oliver et al. (1993) for more
 219 extensive details about the behaviour of ω_R .

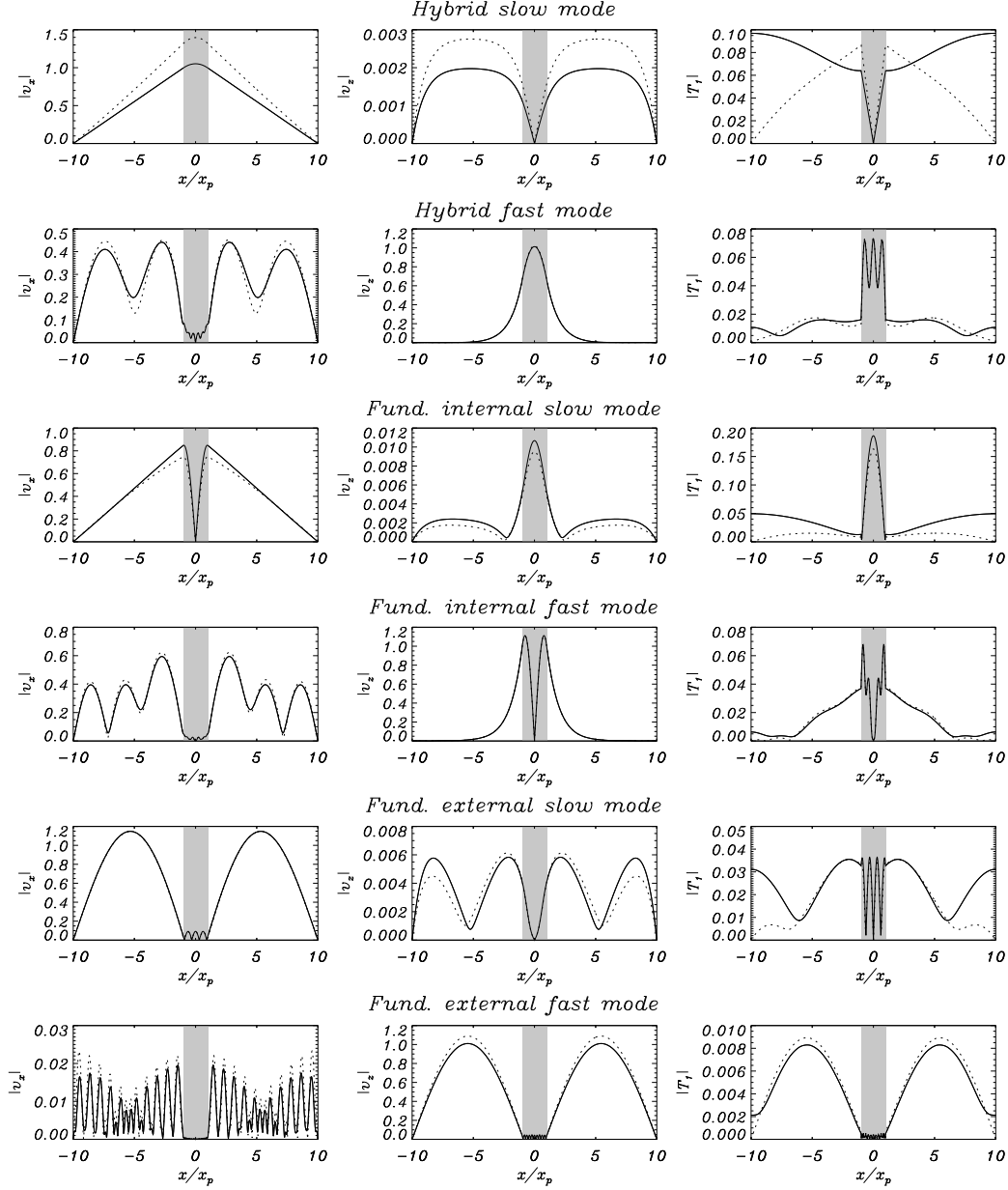


Fig. 3. Modulus of the eigenfunctions v_x , v_z and T_1 (in arbitrary units) versus the dimensionless distance to the slab axis corresponding to the fundamental oscillatory modes for $k_z x_p = 1$. The solid line corresponds to the boundary conditions $v_x = v_z = T_1' = 0$ at $x = \pm x_c$, while the dotted line corresponds to the boundary conditions $v_x = v_z = T_1 = 0$ at $x = \pm x_c$. The shaded region shows the location of the prominence slab.

Next, we focus on the fundamental modes and their eigenfunctions v_x , v_z and T_1 are displayed in Fig. 3 for $k_z x_p = 1$ and for both sets of boundary conditions. The spatial structure of the disturbances v_x and v_z is the one shown by Oliver et al. (1993). Hence, non-adiabatic effects do not modify the spatial behaviour of velocity perturbations. Internal modes produce large plasma

displacements inside the slab, external modes achieve large amplitudes in the corona and the amplitude of hybrid modes is of the same order in both media. It is worth to mention that the hybrid fast mode can be considered as an internal-like mode for large $k_z x_p$ since the amplitude of its perturbations in the corona decreases as $k_z x_p$ increases. Regarding the temperature perturbation, it is larger for the slow modes than for the fast modes and, in general, is larger in the prominence than in the corona. Finally, the differences between the eigenfunctions for the two sets of boundary conditions (Eqs.(6)–(7)) are only relevant for the hybrid slow mode.

From the observational point of view, internal and hybrid modes could be more easily observed than external modes by instruments focusing on prominences, since the amplitude of the latter ones is very small in the prominence body. For this reason, the results corresponding to internal and hybrid modes are the most interesting for prominence seismology. However, here we study the three kinds of solutions in order to perform a complete description of the fundamental wave modes supported by the equilibrium configuration.

3.2 Mode coupling

Oliver et al. (1993) showed that avoided crossings occur in the dispersion diagram when two solutions couple and interchange their magnetoacoustic properties. Nevertheless, no avoided crossings seem to take place in our dispersion diagram (Fig. 2) since the curves of ω_R for the internal fast modes and for the slow modes cut each other. This fact can be understood by considering that in the present, non-adiabatic case the complete dispersion diagram is in a three-dimensional space because the frequency has an imaginary part. So, Fig. 2 actually corresponds to a projection of the complete three-dimensional dispersion diagram on the $k_z \omega_R$ -plane.

Upon exploring the complete dispersion diagram, we have found that three different couplings can take place:

- (1) If the imaginary parts of the frequency of the coupling modes differ by several orders of magnitude, there is no avoided crossing between the real parts. Hence, the coupling between modes is “weak” and only becomes apparent by means of a slight mutual approach of the imaginary parts of ω (see Fig. 4, left panel).
- (2) If both imaginary parts of the frequency have a similar value, the real parts show an avoided crossing and so a “strong” coupling takes place (see Fig. 4, mid panel).
- (3) In very peculiar cases, an “anomalous” coupling takes place when the imaginary parts of ω of the two coupling modes repel each other (see

263 Fig. 4, right panel). This situation has important effects on the wave
 264 stability, as we explain in Sect. 3.5.

265 The behaviour of the mode coupling was previously described by Terradas et al.
 266 (2001) in the cases that we call “weak” and “strong” couplings (compare our
 267 Fig. 4 with Fig. 12 of Terradas et al., 2001).

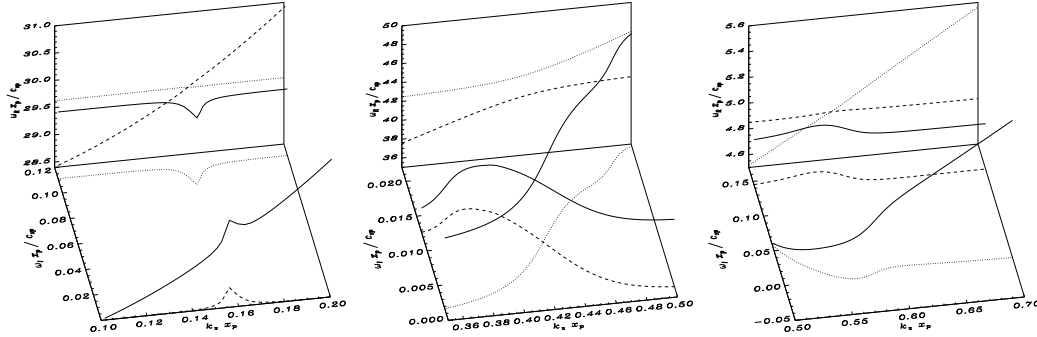


Fig. 4. Three-dimensional dispersion diagrams (solid lines) close to a coupling between a fast mode and a slow mode. Dashed and dotted lines are the projections of the dispersion curves on the horizontal and vertical planes. The left-hand side panel presents a “weak” coupling, the middle panel shows a “strong” coupling and the right-hand side panel displays an “anomalous” coupling.

268 3.3 Periods and damping times

269 Hereafter we restrict ourselves to the fundamental modes and compute the
 270 oscillatory period, P , the damping time, τ_D , and the ratio of the damping
 271 time to the period as functions of the dimensionless wavenumber, $k_z x_p$. We
 272 consider values for $k_z x_p$ between 0.01 and 3, which correspond to wavelengths
 273 between 5×10^3 km and 10^5 km, approximately. These values cover the range of
 274 typically observed wavelengths in prominence oscillations (Oliver & Ballester,
 275 2002). The results of the computations are displayed in Fig. 5 considering the
 276 two sets of boundary conditions (Eqs. (6)–(7)).

277 The periods obtained here agree with those provided and commented by
 278 Joarder & Roberts (1992) and Oliver et al. (1993), therefore we turn our at-
 279 tention to the damping times. Regarding slow modes, we see that they are
 280 strongly damped, with values of τ_D/P close to 1 for the three modes. How-
 281 ever, fast modes are much less attenuated and the obtained values of τ_D/P
 282 are much larger than those observed. This fact involves an important difference
 283 with the results of Paper I, in which fast waves were efficiently attenuated
 284 for some values of the wavenumber. Such as happens with the period, the
 285 damping time of slow modes is almost independent of k_z . On the contrary,
 286 fast modes are less attenuated for small k_z than for large k_z . This evidence
 287 can be understood by means of the following arguments. Considering $k_z = 0$

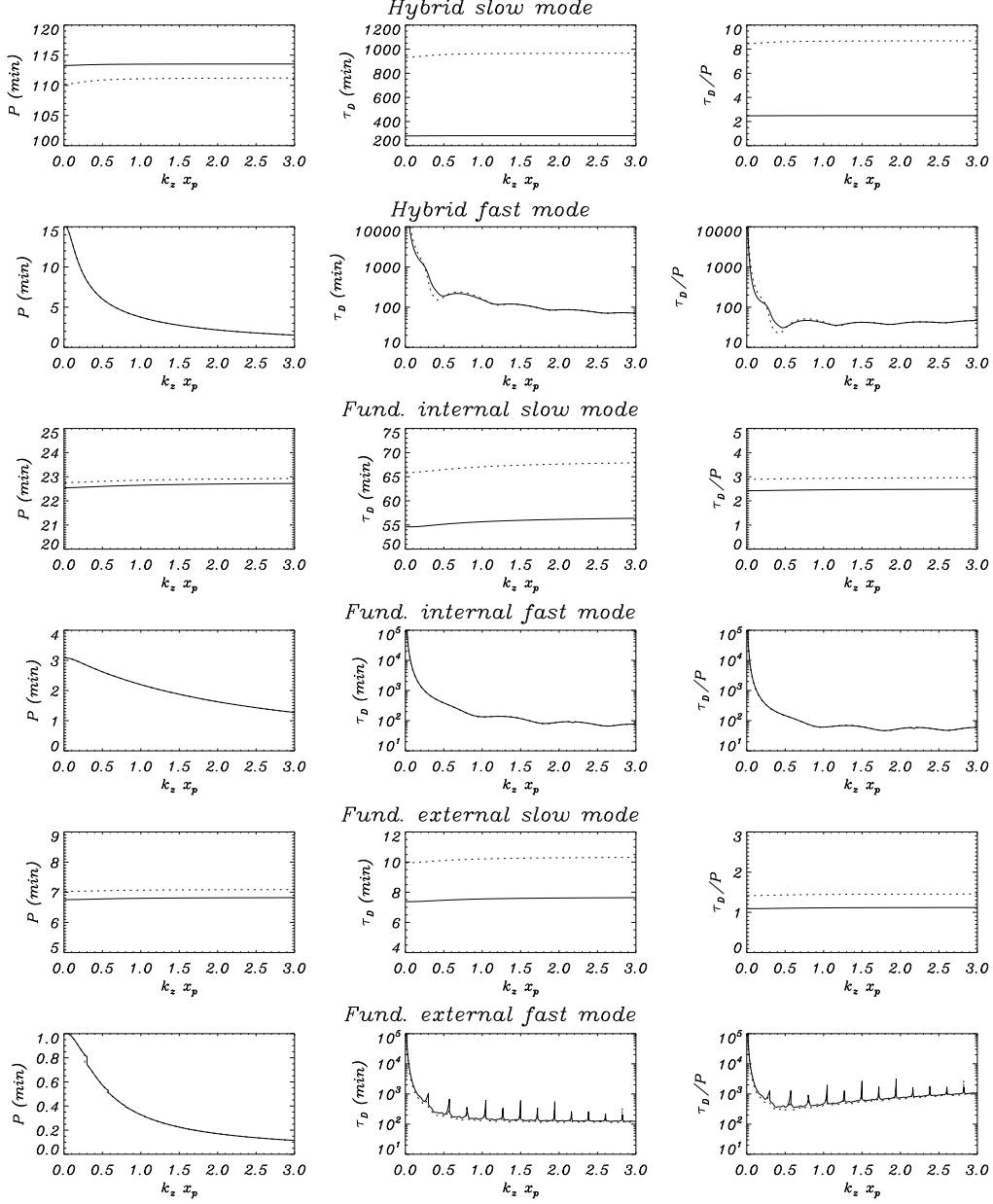


Fig. 5. Period (left), damping time (centre) and ratio of the damping time to the period (right) versus $k_z x_p$ for the fundamental oscillatory modes. The solid line corresponds to the boundary conditions $v_x = v_z = T'_1 = 0$, while the dotted line corresponds to the boundary conditions $v_x = v_z = T_1 = 0$.

288 then Eqs. (2)–(4) become,

$$289 \quad c_s^2 \frac{d^2 v_x}{dx^2} + \gamma \omega^2 v_x - \frac{i \omega c_s^2}{T_0} \frac{dT_1}{dx} = 0, \quad (9)$$

$$290 \quad v_A^2 \frac{d^2 v_z}{dx^2} + \omega^2 v_z = 0, \quad (10)$$

$$\kappa_{\parallel} \frac{1}{p_0} \frac{d^2 T_1}{dx^2} - \left(\omega_T + \frac{i\omega}{\gamma - 1} \right) \frac{T_1}{T_0} - \left(1 + \frac{i\omega_{\rho}}{\omega} \right) \frac{dv_x}{dx} = 0. \quad (11)$$

Equations (9) and (11) are still coupled and govern slow and thermal waves, which are affected by non-adiabatic mechanisms through the terms with κ_{\parallel} , ω_T and ω_{ρ} in Eq. (11). On the contrary, Eq. (10) is now decoupled from the rest and governs fast modes alone, which become pure Alfvén waves and are not affected by non-adiabatic terms. Thus, for $k_z \rightarrow 0$ fast waves tend to the ideal, undamped behaviour. When k_z is increased, fast modes are more affected by acoustic effects and their damping time decreases and stabilises. The little peaks shown in the bottom panels of Fig. 5, corresponding to the external fast mode, are in fact the result of “strong” couplings with slow mode harmonics. The differences arising from the different boundary conditions are only of importance for the hybrid slow mode, as we indicated in Sect. 3.1. We see that the boundary condition $T'_1 = 0$ produces a substantially stronger damping for the hybrid slow mode than the condition $T_1 = 0$.

Finally, an approximate value to the frequency of internal and external slow modes can be obtained by considering the approximation given in App. B of Paper I, namely

$$\omega \approx \Lambda k_x, \quad (12)$$

where k_x is the wavenumber in the field direction and Λ is the modified sound speed due to the presence of non-adiabatic effects, defined in Paper I as follows

$$\Lambda^2 \equiv \frac{c_s^2}{\gamma} \left[\frac{(\gamma - 1) \left(\frac{T_0}{p_0} \kappa_{\parallel} k_x^2 + \omega_T - \omega_{\rho} \right) + i\gamma\omega}{(\gamma - 1) \left(\frac{T_0}{p_0} \kappa_{\parallel} k_x^2 + \omega_T \right) + i\omega} \right]. \quad (13)$$

The value of k_x is fixed by the equilibrium geometry, but for simplicity we consider now the analytical approximations of the dominant wavenumbers given by Joarder & Roberts (1992) in the adiabatic case and for the long wavelength limit, namely

$$k_x \approx \frac{\pi}{2x_p} \quad (14)$$

for the fundamental internal mode, and

$$k_x \approx \frac{\pi}{x_c - x_p} \quad (15)$$

for the fundamental external mode. One must bear in mind that the wavenumbers in the present, non-adiabatic case are complex quantities, but we expect

321 that their real part is similar to that in the adiabatic case, such as happens
 322 with the value of the frequency. Applying now Eq. (12) to the internal slow
 323 mode, i.e. considering prominence parameters in the expression for Λ (Eq. 13)
 324 and the approximation for k_x given by Eq. (14), one obtains $P \approx 23.50$ min,
 325 $\tau_D \approx 73.05$ min and $\tau_D/P \approx 3.11$. On the other hand, if the process is re-
 326 peated for the external slow mode, this gives $P \approx 6.20$ min, $\tau_D \approx 6.70$ min
 327 and $\tau_D/P \approx 1.08$. We see that these approximate values reasonably agree with
 328 those numerically obtained and represented in Fig. 5.

329 3.4 Importance of the damping mechanisms

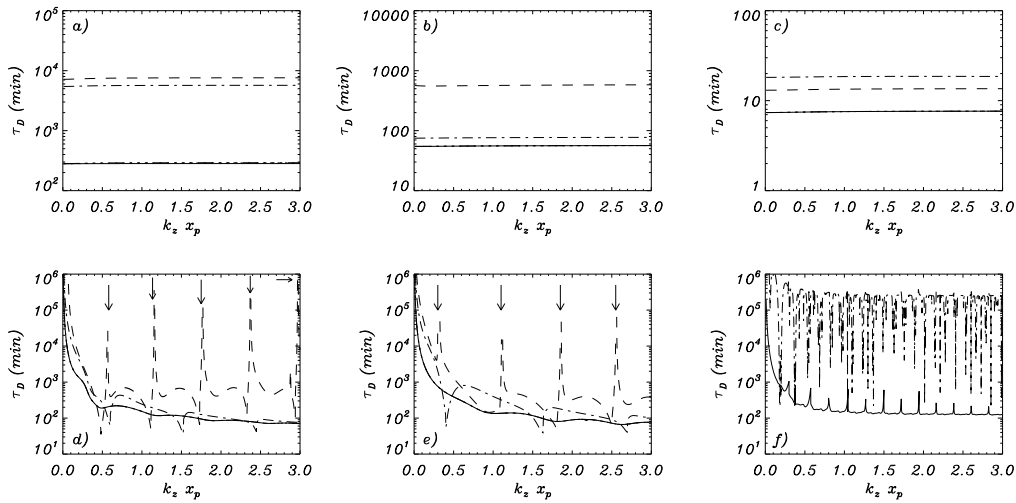


Fig. 6. Damping time versus $k_z x_p$ for the fundamental modes: a) hybrid slow, b) internal slow, c) external slow, d) hybrid fast, e) internal fast, and f) external fast. Different linestyles represent the omitted mechanism: all mechanisms considered (solid line), prominence conduction eliminated (dotted line), prominence radiation eliminated (dashed line), coronal conduction eliminated (dot-dashed line) and coronal radiation eliminated (three dot-dashed line). Arrows in panels d and e point the location of thermal instabilities ($\omega_I < 0$) which appear if prominence radiation is omitted (dashed line).

330 In order to know which are the mechanisms responsible for the damping of
 331 each mode, we now follow the same procedure as in Paper I. We compare the
 332 damping time obtained when considering all non-adiabatic terms (displayed in
 333 the middle column of Fig. 5) with the results obtained when a specific mecha-
 334 nism is removed from the energy equation (Eq. (1)). This analysis allows us to
 335 know whether the omitted mechanism has a relevant effect on the attenuation.

336 Before undertaking this investigation, we need to know if both sets of boundary
 337 conditions are adequate in the absence of thermal conduction. If one imposes

338 $\kappa_{\parallel} = 0$ in Eq. (4) then T_1 can be written as function of v_z and v'_x ,

$$339 \quad T_1 = -\frac{T_0 (1 + i\omega_\rho/\omega)}{\omega_T + i\omega/(\gamma - 1)} (v'_x + ik_z v_z), \quad (16)$$

340 which can be substituted into Eqs. (2) and (3) in order to obtain two coupled
341 differential equations involving the perturbed velocities alone,

$$342 \quad c_s^2 \left(1 + \frac{i\omega}{\hat{\omega}}\right) \frac{d^2 v_x}{dx^2} + \gamma \omega^2 v_x + ik_z c_s^2 \left(1 + \frac{i\omega}{\hat{\omega}}\right) \frac{dv_z}{dx} = 0, \quad (17)$$

$$\begin{aligned} v_A^2 \frac{d^2 v_z}{dx^2} + \left\{ \omega^2 - k_z^2 \left[v_A^2 + \frac{c_s^2}{\gamma} \left(1 + \frac{i\omega}{\hat{\omega}}\right) \right] \right\} v_z \\ + ik_z \frac{c_s^2}{\gamma} \left(1 + \frac{i\omega}{\hat{\omega}}\right) \frac{dv_x}{dx} = 0. \end{aligned} \quad (18)$$

343 Here $\hat{\omega}$ is introduced to simplify the notation,

$$344 \quad \hat{\omega} \equiv \frac{\omega_T + i\omega/(\gamma - 1)}{1 + i\omega_\rho/\omega}.$$

345 Now, the system formed by Eqs. (17) and (18) is fully determined by assuming
346 only boundary conditions for v_x and v_z . Hence, the behaviour of T_1 at the
347 boundaries cannot be imposed but is fixed by the conditions over the velocity
348 perturbations. If one takes $v_x = v_z = T'_1 = 0$ as boundary conditions, then
349 Eq. (16) yields the constraint $v''_x + ik_z v'_z = 0$, which substituted in Eq. (17)
350 automatically gives the redundant condition $v_x = 0$. On the other hand, if
351 one assumes $v_x = v_z = T_1 = 0$ at $x = \pm x_c$, then Eq. (16) now imposes
352 $v'_x = 0$ at the boundaries. This last condition substituted in Eq. (18) gives
353 the extra condition $v''_z = 0$ over the system, which implies a new restriction
354 that is not generally satisfied by all solutions. Thus, $T'_1 = 0$ reveals itself
355 as the “natural” boundary condition for the temperature perturbation when
356 thermal conduction is neglected. So, for the following investigation we restrict
357 ourselves to the boundary conditions $v_x = v_z = T'_1 = 0$ since the conditions
358 $v_x = v_z = T_1 = 0$ are not consistent with the differential equations when
359 thermal conduction is neglected.

360 The results of the computations are displayed in Fig. 6. Although we have
361 explored a wide range of values of k_z , the plots are only drawn again for
362 $0.01 < k_z x_p < 3$ since we have found that the importance of the damping
363 mechanisms does not show a strong dependence on k_z . Regarding slow modes,
364 we clearly see that the damping of the internal mode is dominated by the radi-
365 ation from the prominence plasma, as expected, while coronal conduction has

366 a minor effect. On the other hand, the hybrid and external modes are affected
 367 by coronal conduction together with prominence radiation. Both mechanisms
 368 have a similar influence on the hybrid mode, while coronal conduction domi-
 369 nates the attenuation of the external mode. This result for the hybrid mode
 370 is coherent with the fact that its perturbations achieve large amplitudes both
 371 in the prominence and the corona (see top row of Fig. 3), so one expects that
 372 the most relevant damping mechanisms of each medium govern together the
 373 attenuation of the hybrid mode. However, the result for the external mode is
 374 *a priori* surprising because its perturbations are very small in the prominence
 375 (see fifth row of Fig. 3) and one expects that the prominence-related mecha-
 376 nisms have a minor effect on its damping. The following discussion attempts
 377 to explain why prominence radiation affects so much the external mode.

378 The equilibrium configuration assumed in the present work implies an addi-
 379 tional complication with respect to the equilibrium considered in Paper I, in
 380 which magnetic field lines were taken parallel to the interface between the
 381 prominence and the corona. Hence, both media were thermally isolated in the
 382 model of Paper I since there was no transfer of energy from one medium to the
 383 other. However, in the present model thermal conduction connects both media
 384 since field lines are transverse to the interfaces. This fact allows heat transfer
 385 between the prominence and the corona. So, some energy can flow along field
 386 lines and can be injected from the corona into the prominence, where the en-
 387 ergy is efficiently radiated away by the plasma. In this way, the influence of
 388 prominence radiation on the damping of the external slow mode, and also the
 389 hybrid slow mode, is amplified by means of coronal thermal conduction.

390 Next we turn our attention to the fast modes. At first sight, the behaviour of
 391 the fast modes when a specific mechanism is removed from the energy equation
 392 is absolutely different from that seen in the case of the slow modes and needs
 393 more extensive explanations. In Sect. 3.3, we commented that the damping
 394 time of the fast modes is affected by the couplings with the slow modes.
 395 Now, we see that the nature of these couplings (being “weak”, “strong” or
 396 “anomalous”) changes depending on which is the non-adiabatic mechanism
 397 omitted in the energy equation. These changes in the coupling nature cause
 398 the damping time of the hybrid fast mode and the internal fast mode to vary
 399 from small values to very large values depending on the proximity to the
 400 couplings. So, we see that the consideration of both prominence radiation and
 401 coronal conduction has the effect of smoothing the curves of τ_D .

402 In addition, the results corresponding to hybrid and internal fast modes show
 403 the appearance of thermal instabilities in very localised values of $k_z x_p$ when
 404 prominence radiation is neglected (dashed lines), since then the interactions
 405 between fast modes and external slow modes leads to “anomalous” couplings.
 406 At these couplings, the value of ω_l for the fast modes is pushed towards neg-
 407 ative values (see the right-hand panel of Fig. 4). Such a situation has very

important repercussions on the wave behaviour since for $\omega_I < 0$ waves are amplified in time. The location of these instabilities in panels *d* and *e* of Fig. 6 have been pointed by means of arrows.

3.5 Wave instabilities

Wave instabilities discussed in Sect. 3.4 require a more in-depth investigation. According to Field (1965), the criterion for the appearance of wave instabilities is given by

$$\frac{\kappa_{\parallel}}{\rho_0} k_x^2 + L_T + \frac{1}{\gamma - 1} \frac{\rho_0}{T_0} L_{\rho} < 0, \quad (19)$$

where k_x is the wavenumber in the field direction. Results of Carbonell et al. (2004), see also Paper I, point out that the heating scenario used in our calculations (constant heating per unit volume) cannot lead to thermal destabilisation. So, we can affirm that instabilities described in Sect. 3.4 are not caused by the heating mechanism. In addition, instabilities only appear when radiative losses are omitted. In such situation, the instability criterion becomes

$$\frac{\kappa_{\parallel}}{\rho_0} k_x^2 < 0. \quad (20)$$

Equation (20) is never satisfied unless an additional source of heating is present, which seems to be the present case. This extra energy source corresponds to heat injected from the corona into the prominence by thermal conduction, as was commented in Sect. 3.4. In the absence of radiation, prominence thermal conduction is the only mechanism that can dissipate this extra injected heat. One expects that in such situation the value of k_x grows in order to increase the efficiency of prominence conduction. Figure 7 shows the eigenfunction of the temperature perturbation corresponding to the internal fast mode for $k_z x_p \approx 0.3$ when all non-adiabatic mechanisms are considered, panel *a*), and when radiative losses from the prominence plasma are omitted, panel *b*). For this value of $k_z x_p$, the wave becomes unstable ($\omega_I < 0$) if prominence radiation is omitted. We see that smaller spatial-scales (i.e. larger k_x) are obtained within the prominence when prominence radiation is not taken into account, as expected. Although the efficiency of prominence conduction is increased in this way, it is still not enough to stabilise the perturbation.

This last discussion points out that prominence radiative losses are of paramount importance to stabilise the disturbances. The efficiency of prominence radiation can be quantified by means of the radiation time-scale for the prominence

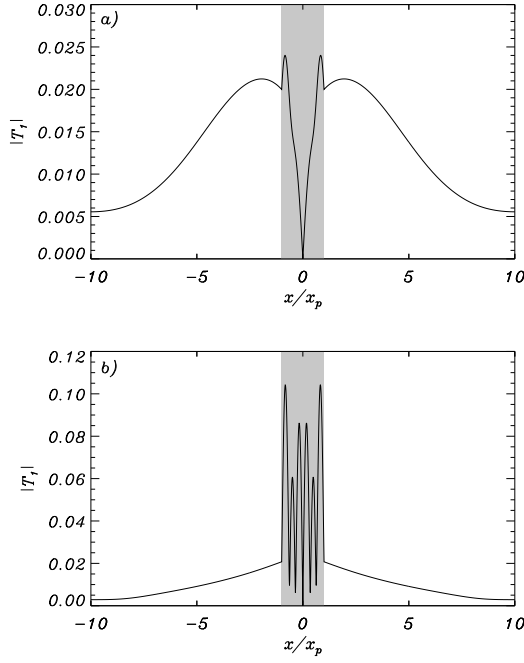


Fig. 7. Modulus of the eigenfunction T_1 (in arbitrary units) versus the dimensionless distance to the slab axis corresponding to the fundamental internal fast mode for $k_z x_p \approx 0.3$ if a) all non-adiabatic mechanisms are considered, and b) without prominence radiation. The shaded region shows the location of the prominence slab.

441 plasma (De Moortel & Hood, 2004),

$$442 \quad \tau_r = \frac{\gamma p_0}{(\gamma - 1) \rho_p^2 \chi_p^* T_p^{\alpha_p}}. \quad (21)$$

443 Considering fixed equilibrium parameters, the value of τ_r changes for different
 444 optical thicknesses of the prominence material (see regimes listed in Table I
 445 of Paper I). For Prominence (1) parameters (optically thin plasma), $\tau_r \approx$
 446 309 s, whereas for Prominence (2) and Prominence (3) regimes (optically thick
 447 and very thick plasma), $\tau_r \approx 2,876$ s and $\tau_r \approx 47,822$ s, respectively, and so
 448 prominence radiation is less efficient. Obviously, $\tau_r \rightarrow \infty$ if the radiative term
 449 is omitted. The coronal plasma is always taken optically thin. Figure 8 shows
 450 the damping time of the fundamental hybrid and internal fast modes as a
 451 function of $k_z x_p$ for the different prominence optical regimes. We see that
 452 the larger the optical thickness, the larger the damping time. This effect is
 453 especially relevant at the coupling points with the external slow modes, where
 454 thermal instabilities appear if radiative losses are completely inhibited.

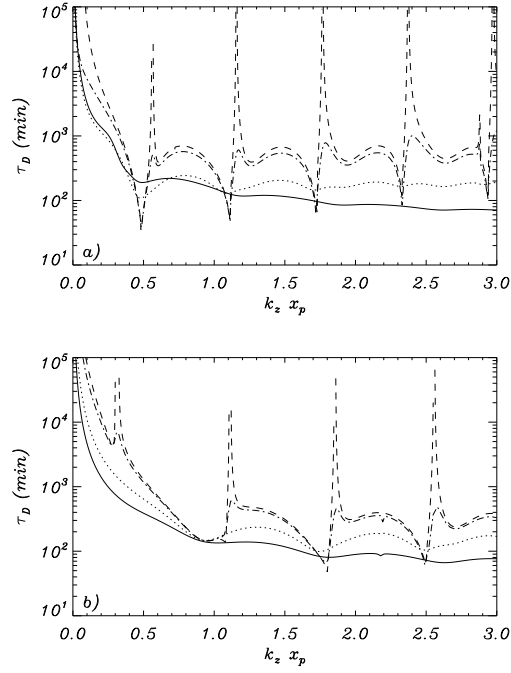


Fig. 8. Damping time versus $k_z x_p$ for the fundamental *a*) hybrid and *b*) internal fast modes. The linestyles represent different optical thicknesses for the prominence plasma: Prominence (1) in solid line (this corresponds to the solid lines in Fig. 6*d* and *e*), Prominence (2) in dotted line and Prominence (3) in dot-dashed line. The dashed line corresponds to the results when the prominence radiation is omitted (dashed lines in Fig. 6*d* and *e*). The boundary conditions considered are $v_x = v_z = T'_1 = 0$.

3.6 Exploring the parameter space

In this Section we investigate how the attenuation of oscillations is affected by changing the equilibrium parameters. The motivation of this study is based on the fact that the estimated values for prominence plasma parameters, such as temperature, density, magnetic field strength or optical thickness, varies from one prominence to another, sometimes in a significant way (e.g. Patsourakos Vial, 2002). Thus, it is important for our investigation to ascertain the sensitivity of the damping time to the equilibrium parameters around the values considered in our previous calculations.

First, we plot in Fig. 9 the ratio of the damping time to the period corresponding to the fundamental modes as a function of equilibrium physical conditions, namely the prominence temperature, the prominence density, the magnetic field strength and the coronal temperature. The following ranges of values have been considered: $5000 \text{ K} < T_p < 15,000 \text{ K}$; $10^{-11} \text{ kg m}^{-3} < \rho_p < 10^{-10} \text{ kg m}^{-3}$; $1 \text{ G} < B_0 < 15 \text{ G}$; and $800,000 \text{ K} < T_c < 2,000,000 \text{ K}$.

At first sight, we notice that the attenuation of fast modes is much more

471 sensitive to the equilibrium conditions than the damping of slow modes. The
 472 attenuation of slow modes does not change in a significant way if the equi-
 473 librium physical conditions are modified, since the obtained τ_D/P are always
 474 small and of the same order of magnitude. On the contrary, fast modes are
 475 highly sensitive especially to the prominence density and the magnetic field. It
 476 is noticeable that small values of τ_D/P are obtained for the fast modes when
 477 large densities and weak magnetic fields are considered. If the magnetic field
 478 strength is increased or the prominence density is reduced, then τ_D/P grows
 479 dramatically. Additionally, fast modes are again strongly affected by the cou-
 480 plings with slow modes, a fact that shows up in the form of very localised
 481 increases and decreases of τ_D/P .

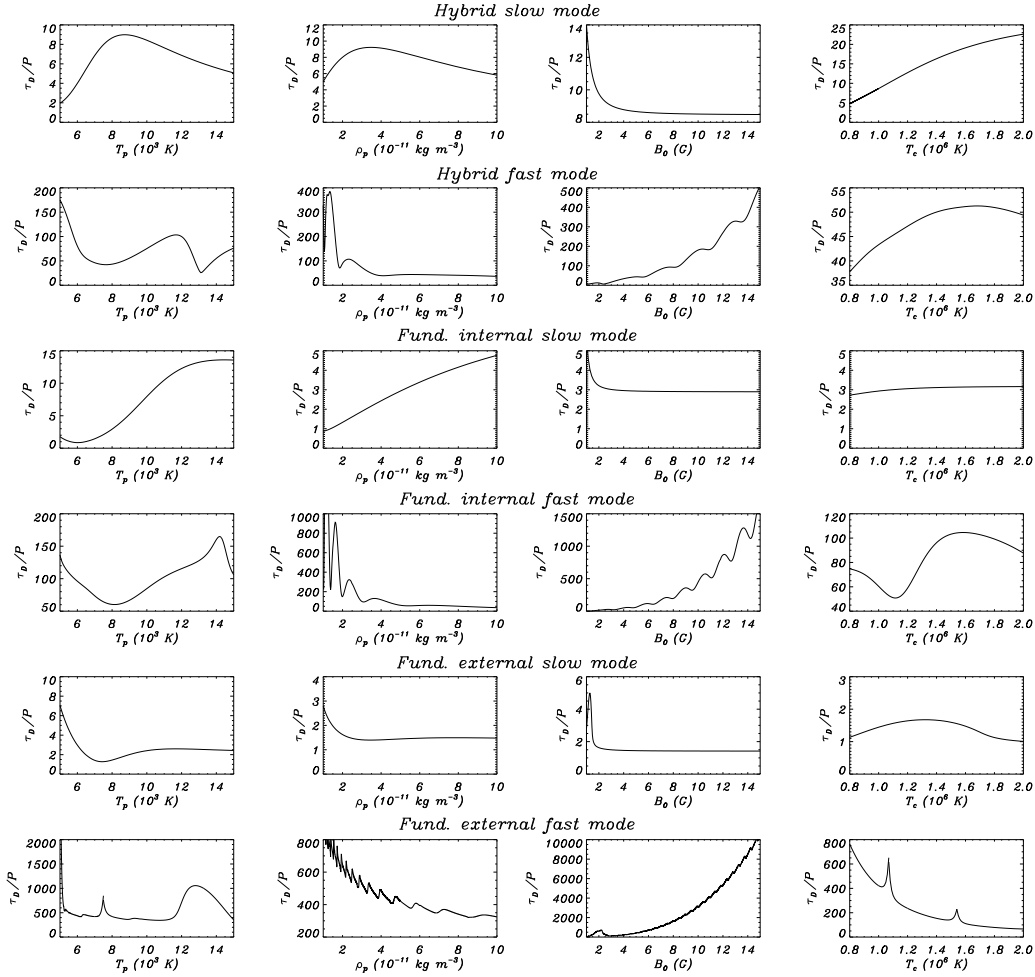


Fig. 9. Ratio of the damping time to the period for the fundamental oscillatory
 modes as function of, from the left to the right, the prominence temperature,
 the prominence density, the magnetic field strength and the coronal tempera-
 ture. Computations performed considering $k_z x_p = 1$ and the boundary conditions
 $v_x = v_z = T_1 = 0$ at $x = \pm x_c$.

482 On the other hand, we have studied the effect of considering a different heating
 483 scenario on the wave attenuation. In agreement with previous investigations

484 (Carbonell et al., 2004; Terradas et al., 2005), results do not show significant
 485 discrepancies if different heating mechanisms are assumed.

486 Finally, we have also varied the length of magnetic field lines (by modifying
 487 the value of x_c) and the prominence half-width, x_p , in order to assess their
 488 effect on the damping time. For realistic values of both x_c and x_p , no significant
 489 influences appear in the results with respect to those previously discussed. It is
 490 worth to mention that prominence conduction becomes a relevant mechanism
 491 for very a small, unrealistic prominence half-width ($x_p \lesssim 10$ km), and coronal
 492 radiation is only important for very large, and again unrealistic, length of
 493 magnetic field lines ($x_c \gtrsim 10^6$ km).

494 3.7 Comparison with Terradas et al. (2005)

495 The final check of the importance of the coronal medium comes from the com-
 496 parison between our results and those obtained by Terradas et al. (2005) in
 497 the case of an isolated prominence slab (see Fig. 10). Obviously, this com-
 498 parison can only be performed for internal modes, since external and hybrid
 499 modes are not supported by an isolated slab. The boundary conditions as-
 500 sumed in the work of Terradas et al. (2005) are $v_x = v_z = T'_1 = 0$. According
 501 to the arguments given in Sect. 3.4, this condition for the perturbation to
 502 the temperature is the most suitable since thermal conduction is negligible
 503 in prominences. However, the line-tying condition at the edges of the promi-
 504 nence slab seems not to be the most appropriate election in the light of the
 505 eigenfunctions plotted in Fig. 3. Hence, our results point out that the interface
 506 between the prominence slab and the corona does not act as a rigid wall, and
 507 perturbations can be important in the corona even for internal modes.

508 Contrary to what was shown in Paper I, in which only the fast mode was
 509 affected by the corona, in the present case both slow and fast modes of the
 510 isolated slab differ from those of a prominence–corona equilibrium. A decre-
 511 ment of the damping time is obtained for both waves in comparison with
 512 the solution of an isolated slab. The slow mode is less affected by the pres-
 513 ence of the corona but the fast mode damping time is reduced by an order of
 514 magnitude, although it is still far from the observed values. As in the longi-
 515 tudinal magnetic field case, the consideration of the corona is of paramount
 516 importance for a correct description of the behaviour of oscillations and their
 517 attenuation, although its effect on the damping of fast modes is less noticeable
 518 than in the longitudinal case.

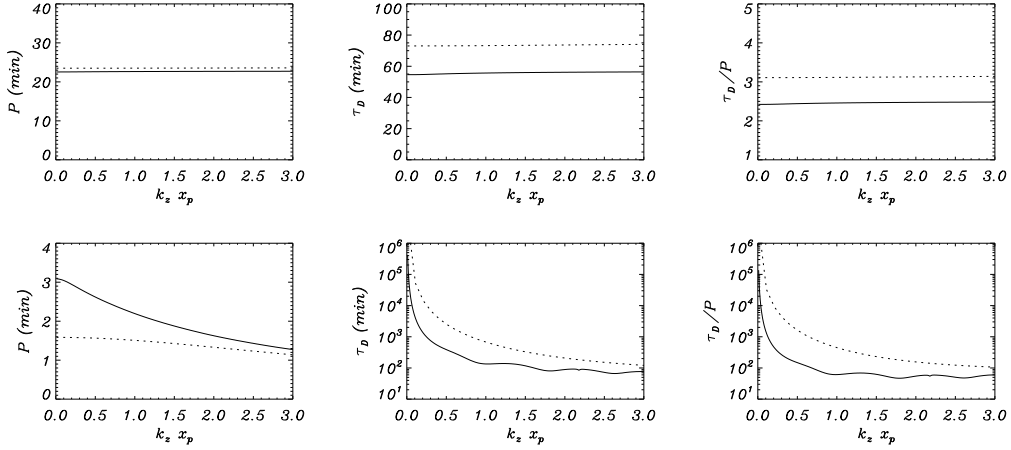


Fig. 10. Period (left), damping time (centre) and ratio of the damping time to the period (right) versus k_z for the internal fundamental slow (upper panels) and fast (bottom panels) oscillatory modes. The solid lines are the solutions of a prominence plus corona equilibrium whereas the dotted lines represent the solutions of an isolated slab (Terradas et al., 2005).

4 Conclusions

In this paper we have studied the wave attenuation in a system representing a quiescent solar prominence embedded in the coronal medium. The prominence has been modelled as a homogeneous plasma slab surrounded by a homogeneous medium with coronal conditions. Magnetic field lines have been assumed transverse to the prominence slab axis and the whole system has been bounded in the field direction by two photospheric rigid walls, in order to establish a realistic length for the field lines. The attenuation of the normal modes of such equilibrium has been investigated by considering parallel thermal conduction, radiative losses and plasma heating as non-adiabatic mechanisms, and focusing our study on the fundamental oscillatory modes. The main conclusions of this work are summarised next.

- (1) Slow modes are strongly attenuated by non-adiabatic mechanisms, their damping times being of the order of the corresponding periods. Fast modes are less affected and present greater damping times.
- (2) The most relevant damping mechanisms are prominence radiation and coronal thermal conduction. The first one dominates the damping of internal modes, while the second one is responsible for the attenuation of external modes. The combined effect of both mechanisms governs the damping of hybrid modes. Neither prominence conduction nor coronal radiation become of importance for realistic values of the length of magnetic field lines and the prominence width.
- (3) The attenuation of slow modes is not affected by the value of the free

component of the wavenumber, k_z . On the contrary, the behaviour of fast modes is strongly dependent on k_z .

- (4) Thermal conduction allows energy transfer between the prominence slab and the coronal medium. Prominence radiation has an essential role in dissipating the extra heat injected from the corona and stabilises the oscillations. Thermal instabilities appear if the radiative losses from the prominence plasma are omitted or significantly reduced (e.g. caused by an increase of the optical thickness) since the plasma cannot dissipate the extra injected heat in an efficient way.
- (5) The damping time of fast modes is strongly sensitive to the equilibrium physical parameters while slow waves are less affected by the variation of the equilibrium conditions.
- (6) The presence of the corona produces a decrement of the damping time of internal modes with respect to the solutions supported by an isolated prominence slab. Nevertheless, this effect is not enough to obtain damping times of the order of the period in the case of fast modes.

Considering the equilibrium parameters of Paper I, the efficiency of non-adiabatic mechanisms on the damping of fast modes is smaller in the present case. This fact suggests that the orientation of magnetic field lines with respect to the slab axis has a relevant influence on the attenuation of fast modes, the configuration of Paper I and the present one being limit cases. Moreover, fast modes are strongly sensitive to the equilibrium physical conditions, and it is possible to obtain small values of the damping time by considering extreme equilibrium parameters, such as very weak magnetic fields and very large prominence densities. In this way, fast modes show a wide range of theoretical damping times. On the other hand slow modes are always efficiently attenuated, with damping times of the order of their periods. This result suggests that the attenuation of prominence fast waves may be caused by other damping mechanisms not considered here. Some candidates could be resonant absorption (Arregui et al., 2008) and ion-neutral collisions (Forteza et al., 2007). Among these mechanisms, resonant absorption may be a very efficient damping mechanism if non-uniform equilibria are considered, e.g. models with a transition region between the prominence and the corona. Other effects, as wave leakage, might only play a minor role in the damping of disturbances. Finally, future studies should take into account the prominence fine structure on the basis that small-amplitude oscillations are of local nature. Therefore, the investigation of the damping of fibril oscillations should be the next step.

R. O. and J. L. B. want to acknowledge the International Space Science Institute teams “Coronal waves and Oscillations” and “Spectroscopy and Imaging of quiescent and eruptive solar prominences from space” for useful discussions. The authors acknowledge the financial support received from the Spanish MCyT and the Conselleria d’Economia, Hisenda i Innovació of the CAIB under Grants No. AYA2006-07637 and PCTIB-2005GC3-03, respectively. Fi-

nally, R. S. thanks the Conselleria d'Economia, Hisenda i Innovació for a fellowship.

References

- Anzer, U. & Heinzl, P. 1999, *A&A*, 349, 974
- Arregui, I., Terradas, J. Oliver, R., & Ballester, J. L. 2008, *ApJ*, 682, L141
- Ballai, I. 2003, *A&A*, 410, L17
- Ballester, J. L. 2006, *Phil. Trans. R. Soc. A*, 364, 405
- Balthasar, H., Wiehr, E., Schleicher, H., & Wöhl, H. 1993, *A&A*, 277, 635
- Banerjee, D., Erdélyi, R., Oliver R., & O'Shea, E. 2007, *Sol. Phys.*, 246, 3
- Berger, T. E. 2008, *ApJ*, 676, L89
- Carbonell, M., Oliver, R., & Ballester, J. L. 2004, *A&A*, 415, 739
- Carbonell, M., Terradas, J., Oliver, R., & Ballester, J. L. 2006, *A&A*, 460, 573
- Cargill, P. & Hood, A. W. 1989, *Sol. Phys.*, 124, 101
- Dahlburg, R. B. & Mariska, J. T. 1988, *Sol. Phys.*, 117, 51
- De Moortel, I. & Hood, A. W. 2004, *A&A*, 415, 705
- Field, G. B. 1965, *ApJ*, 142, 531
- Forteza, P., Oliver, R., Ballester, J. L., & Khodachenko, M. L. 2007, *A&A*, 461, 731
- Foullon, C., Verwichte, E., & Nakariakov, V. M. 2004, *A&A*, 427, L5
- Harvey, J. 1969, Ph.D. thesis, University of Colorado, USA
- Goedbloed, H. & Poedts, S. 2004, *Principles of magnetohydrodynamics*, Cambridge University Press
- Hildner, E. 1974, *Sol. Phys.*, 35, 123
- Joarder, P. S. & Roberts, B. 1992, *A&A*, 261, 625
- Kippenhahn, R. & Schölter, A. 1957, *Z. Astrophys.*, 43, 36
- Lin, Y. 2004, P.h. D. Thesis, University of Oslo
- Low, B. C. & Wu, S. T. 1981, *ApJ*, 248, 335
- Menzel, D. H. 1951, *AJ*, 56, 135
- Milne, A. M., Priest, E. R., & Roberts, B. 1979, *ApJ*, 232, 304
- Molowny-Horas, R., Wiehr, E., Balthasar, H. et al. 1999, *JOSO Annual Report 1998*, Astronomical Institute Tatranska Lomnica, 126
- Ofman, L. & Wang, T. J. 2008, *A&A*, 482, L9
- Okamoto, T. J, et al. 2007, *Science*, 318, 1557
- Oliver, R., Ballester, J. L., Hood, A. W., & Priest, E. R. 1993, *ApJ*, 409, 809
- Oliver, R. & Ballester, J. L. 1996, *ApJ*, 456, 393
- Oliver, R. & Ballester, J. L. 2002, *Sol. Phys.*, 206, 45
- Patsourakos, S & Vial, J.-C. 2002, *Sol. Phys.*, 208, 253
- Poland, A & Anzer, U. 1971, *Sol. Phys.*, 19, 401
- Porter, L. J., Klimchuk, J. A., & Sturrock, P. A. 1994, *ApJ*, 435, 482
- Rosner, R., Tucker, W. H., & Vaiana, G. S. 1978, *ApJ*, 220, 643
- Schutgens, N. A. J. 1997a, *A&A*, 323, 969

626 Schutgens, N. A. J. 1997b, A&A, 325, 352
 627 Schutgens, N. A. J., Tóth, G. 1999, A&A, 345, 1038
 628 Sewell, G. 2003, Finite Differences, Finite Elements and PDE2D
 629 Soler, R., Oliver, R., & Ballester, J. L. 2007, A&A, 471, 1023 (Paper I)
 630 Terradas, J., Oliver, R., & Ballester, J. L. 2001, A&A, 378, 635
 631 Terradas, J., Molowny-Horas, R., Wiehr, E. et al. 2002, A&A, 393, 637
 632 Terradas, J., Carbonell, M., Oliver, R., & Ballester, J. L. 2005, A&A, 434, 741
 633 Terradas, J., Arregui, I., Oliver, R., & Ballester, J. L. 2008, ApJ, 678, L153